Mechanical Systems and Signal Processing 179 (2022) 109339

Contents lists available at ScienceDirect

Mechanical Systems and Signal Processing

journal homepage: www.elsevier.com/locate/ymssp

A generalization of the Valanis model for friction modelling

Hassan Jalali [a,*], Nidhal Jamia [b], Michael I. Friswell [b], Hamed Haddad Khodaparast [b], Javad Taghipour [b]

[a] Department of Mechanical and Construction Engineering, Northumbria University, Newcastle Upon Tyne NE1 8ST, UK
[b] Faculty of Science and Engineering, Swansea University, Bay Campus, Fabian Way, Crymlyn Burrows, Swansea SA1 8EN, UK

ARTICLE INFO

Communicated by John E. Mottershead

Keywords:
Frictional contact interface
Hysteresis loop
Bolted joint

ABSTRACT

The complex dynamics of a frictional contact interface have been the subject of many research investigations. However, a comprehensive model has not been proposed that can be easily solved and considers the effect of all parameters of interest, i.e., the variation in contact pressure, the interaction of normal and tangential direction mechanisms, and contact surface degradation. This paper proposes a generalized slip model based on the original Valanis model with the ability to generate non-symmetric hysteresis loops for frictional contact interface modelling and identification. Various numerical and simulation results are used to show the capability of the generalized Valanis model. The advantages of the model presented in this paper are its simplicity and accuracy. The model offers an explicit solution for the Hysteresis loop and is Lipschitz continuous, making it an ideal choice for real-time analyses, such as in digital twins' applications. The model can represent both point-to-point contacts in a joint interface and the joint interface as a whole. The latter application is considered in this paper.

1. Introduction

Friction is a well-known phenomenon that occurs between two surfaces in contact, and often is the main source of damping in assembled structures due to the presence of bolted joints. Therefore, the contribution of frictional joints can be very significant in the dynamic response of a structure. Furthermore, the friction leads to a continuous variation of the contact conditions under harmonic loading. This makes the analysis of the joint contact very challenging. Therefore, predicting the dynamic response of an assembled structure has been a well-known challenge for researchers in the last four decades.

Previous models proposed for the frictional contact interface in joints usually are governed by complicated nonlinear differential equations. This makes these models less useful in terms of analysis cost in applications such as digital twins, where a full model (or a part model) of a structure containing many joints is constructed. Friction models providing both accuracy in predicting the contact interface's detailed dynamics and simplicity in being solved and analysed with less effort are best fit for this purpose.

The friction force in a contact interface is a function of the relative velocity between the surfaces. Generally, this function is mainly related to the sliding direction of the two contacting surfaces, thus neglecting any contribution of the normal components of the contact force to the contact interface dynamics. Researchers categorize the joint models as rate-dependent and rate-independent. This categorization depends on whether the model can be written in a form independent or dependent on the velocity magnitude.

Known for its relatively simple mathematical model, the Bouc-Wen model is one of the most popular rate-independent hysteretic

* Corresponding author.
E-mail address: Hassan.jalali@Northumbria.ac.uk (H. Jalali).

https://doi.org/10.1016/j.ymssp.2022.109339
Received 10 January 2022; Received in revised form 24 April 2022; Accepted 20 May 2022
Available online 30 May 2022

semi-physical models. It was proposed by Bouc in 1971 [1–2] and generalized by Wen in 1976 [3]. They introduced a model that captures both the linear elastic and elasto-plastic restoring forces and relates it to the input displacement in a hysteric way. Ismail et al. [4] provided a review of the different developments and implementations of the Bouc-Wen model. Ni et al. [5] developed a frequency domain method to identify Bouc-Wen differential model parameters of non-linear hysteretic isolators using experimental data from periodic vibration tests. Oldfield et al. [6] introduced the four-parameter Bouc-Wen model to analyze the dynamic frictional contact of a bolted joint under harmonic loads. The model showed good efficiency in the transition from the microslip to the macroslip behaviour in the joint. An extended Bouc-Wen model was proposed by Sireteanu et al. [7] to improve the capability of the model to predict experimental symmetric hysteretic loops. The applicability of the developed model was illustrated for seismic protection devices. Zhu and Lu [8] introduced the normalized Bouc-Wen model to model a mild steel damper. Using experimental data, the accuracy of the approach was demonstrated. Zaman and Skider [9] used a modified firefly algorithm to identify Bouc-Wen hysteresis model parameters. They showed that the proposed algorithm is well suited for Bouc-Wen hysteresis model parameter identification. Similarly, Ortiz et al. [10] identified the parameters of the Bouc-Wen model but using the Transitional Markov Chain Monte Carlo approach. They accurately estimated the response of the system; however, the estimation of the exact values of the model parameters was not possible. More recently, Noel et al. [11] considered a Bouc-Wen system with a single degree of freedom to analyze the applicability of state-space models to hysteresis identification. They demonstrated the fitting accuracy of the considered approach. Moreover, the Bouc-Wen model exhibits a few drawbacks such as the difficulty of model calibration due to the non-physical aspects of the model parameters [12] that make it difficult to relate the stick–slip behaviour at the joint interface with the model parameters. In addition, the presence of displacement drift and the non-closure of minor loops results in a contradiction with some common plasticity assumptions [13].

While rate-independent models contribute to understanding mathematical models of hysteresis, the rate-dependent models were developed to simulate a wider range of physical effects that arise in the joint contacts [13].

Dahl investigated friction modelling and proposed a simple dynamic model with one state based on the bristle approach [14–15]. This model failed to predict the stick–slip motion due to the difficulty of capturing the Stribeck effect. To overcome this challenge, an extension of the Dahl friction formulation was performed to obtain the well-established LuGre friction force model. This rate-dependent model was the result of a collaboration between the control groups at Lund and Grenoble universities [16] and inspired many other rate-dependent variants. This model is known as a powerful approach to model the frictional contact in mechanical systems. It showed a good ability to capture the Stribeck effect and thus describe the stick–slip motion. The model contains several parameters, and therefore it can simply be matched to the experimental data [17–18]. Do et al. [19] investigated several simulation strategies to apply to dynamic systems with LuGre friction and found that the Runge-Kutta method gave better accuracy. Astrom and de Wit [20] reviewed the properties of the LuGre model, including invariance and zero-slip displacement. They showed that the LuGre model captures many properties of real friction behaviour, but it does not have reversal point memory. Koopman et al. [21] introduced a port-Hamiltonian formulation of the LuGre friction model to be used as a building block in the physical modelling of systems with friction. A quarter-car system with a LuGre-based tyre force model was presented as an example. Jin et al. [22] adopted a LuGre friction model to describe the friction behaviour of a Duffing oscillator. They proposed an analytical technique to evaluate the random response of dynamic friction system with nonlinear stiffness. A friction-induced mechanical oscillator with cubic nonlinearity was analyzed by Pikunov and Stefanski [23]. They applied a modified LuGre friction model to model the friction force, and a stable correlation was obtained between the response of the frictional oscillator and the dynamics of the friction force generated during the motion. Zhou et al. [24] proposed a new parameter identification method for the LuGre model. The modelling method was verified using a wheel mechanism with single-point contacts and multi-point contacts. However, the LuGre model was derived based on the assumption of a constant normal load [16]. Therefore, this friction force model exhibits many numerical difficulties in the case where the contact interface includes an important variation in the normal loads. Marques et al. [25] revisited the LuGre friction force model to overcome those limitations.

Using the mentioned above models with the presence of several joints in the same structure makes the modelling cost very high due to the number of parameters that need to be identified. To overcome this limitation, the Valanis model [26–27], which is considered as one of the most powerful models to treat frictional contact, need fewer parameters to define the frictional contact interface. Gaul and Lenz [28] showed that the Valanis model is able to analyse the dynamic response of a complicated structure with many bolted joints with a significant reduction of the computation cost. The Valanis model showed good potential for capturing the micro-slip and macro-slip behaviour using a single model and simulating the response under harmonic loads [29]. A 3 parameter Coulomb joint model consisting of two linear spring elements and a slider element was used by Gaul et al. [30]. This model predicts the measured hysteresis loops when used for node-to-node contact in a detailed FE model. Ahmadian et al. [31] investigated the dynamic characteristics of a beam with frictional contact support subjected to a constant normal load. The contact interface was simulated based on the Valanis model and the contact parameters were identified using the force state map at a measured vibration level. It was shown that the proposed model could accurately regenerate frictional forces at different measured vibration levels. Jalali et al. [32] considered the identification of a nonlinear contact interface at the boundary of a clamped beam. They used a Valanis model to model the frictional force in the contact interface and showed a good agreement between the experimental and identified hysteresis loops to show the potential of the Valanis model. Abad et al. [33] performed numerical and experimental analyses of a bolted lap joint subjected to varying bolt preloads. They used curve fitting of simulated hysteresis cycles to identify the Valanis model parameters and the effect of the preload variation on these parameters. The use of the Valanis model was experimentally validated.

Several identification methods have been used to model the dynamic behaviour of the jointed structures [34–38]. Ahmadian and Jalali [35–36] identified bolted lap joint model parameters by minimizing the difference between the model predictions and the experimentally measured data. A nonlinear state-space identification approach was introduced by Noel et al. [11] to estimate the

hysteresis dynamics. Naraghi and Nobari [37] proposed an identification procedure based on the concept of the optimum equivalent linear frequency response function to model the nonlinear behaviour of a bolted joint. Jalali et al. [38] applied the force-state mapping technique in the identification of nonlinear lap-jointed structures. In joint modelling, a common assumption used in the original friction models (i.e. Valanis [26], LuGre [16], and Bouc-Wen [1–3] models) states that the contact interface condition remains unchanged during a full cycle of vibration. This assumption, which results in a symmetric hysteresis loop for these models, is not valid for all contact interfaces. Particularly, when micro-vibro-impacts [32] or micro-opening-closing occurs in the contact interface, changing both the contact area and the interfacial contact pressure repeatedly can lead to unsymmetric hysteresis loops and therefore, more suitable slip models should be used to capture the interfacial dynamics.

Over the past decade, the researchers have made several attempts to consider the normal force variation in the contact interface in the original slip models or to propose modified versions of the original slip models, which were reviewed in state of the art. In this paper, a generalized Valanis model based on the original Valanis model is proposed following an investigation of the characteristic of the original Valanis model. An identification approach is proposed and verified using different numerical examples. Furthermore, a 3D detailed model of bolted flange joint is considered to obtain the nonlinear dynamic response of the system which is then used to identify the generalized Valanis model.

In a joint contact interface, the friction force or slip mechanism is a function of contact pressure. Therefore, the change in contact pressure directly affects the contact mechanism in the tangential direction. The contact pressure distribution depends upon the surface roughness quality and surface texture. Contact surface degradation due to the slip mechanism changes the surface roughness quality and may affect the contact pressure distribution. These are regarded as the interaction between tangential and normal contact interface mechanisms. The model proposed in this paper does not directly consider this interaction. A feature of this interaction on the contact interface dynamics is non-symmetric hysteresis loops which can be simulated by the generalized Valanis model proposed in this paper.

This paper is organized in 4 main parts. In Section 2 the characteristics of the original Valanis model are investigated and the generalized Valanis model is proposed in addition to an identification approach based on the generalized Valanis model. In Section 3, four numerical examples are used to verify the proposed identification approach. In Section 4, FE and mathematical models of bolted joint flanges are introduced to analyse the dynamic response of a beam system. Finally in Section 5 the results are discussed, and a linear parameter identification and a nonlinear dynamic analysis are performed.

2. Modelling the hysteretic behaviour

In this section, the original Valanis model is considered as a base and a friction model capable of generating unsymmetric hysteresis loops is proposed. Some characteristics of the original Valanis model are also investigated in this section.

2.1. The original Valanis model

In this section, the original Valanis model and its main properties are investigated. Before discussing the Valanis model properties, it is worth mentioning that the numerical results presented in this section are obtained using the SDOF system shown in Fig. 1.

The restoring force F_{nl} of the nonlinear element NL in Fig. 1 is governed by a Valanis model. The differential equations governing the vibration of the SDOF system and the nonlinear restoring force can be represented as,

$$m\ddot{x} + kx + F_{nl}(t) = F\sin(\omega t) \tag{1}$$

$$\dot{F}_{nl} = E_0\dot{x}\frac{1 + \frac{\lambda}{E_0}sign(\dot{x})(g_1(x) - F_{nl})}{1 + \kappa\frac{\lambda}{E_0}sign(\dot{x})(g_2(x) - F_{nl})}, \lambda = \frac{E_0}{\alpha_0\left(1 - \kappa\frac{E_t}{E_0}\right)} \tag{2}$$

where E_0 is the stiffness of contact interface at the sticking condition, E_t is the slope of hysteresis loop in slip motion, κ controls the transition of the hysteresis loop from stick to slip and λ is characterized by the stick limit. State-dependent functions $g_1(x)$ and $g_2(x)$ are introduced in Equation (2). These functions help to investigate some properties of the Valanis model and to propose the generalized Valanis model later in this section. The function $g_1(x)$ controls the behaviour of the contact interface after the microslip regime and $g_2(x)$ has a very marginal effect on the shape of the Hysteresis loops. In the original Valanis model, we have $g_1(x) = g_2(x) = E_t x$, which

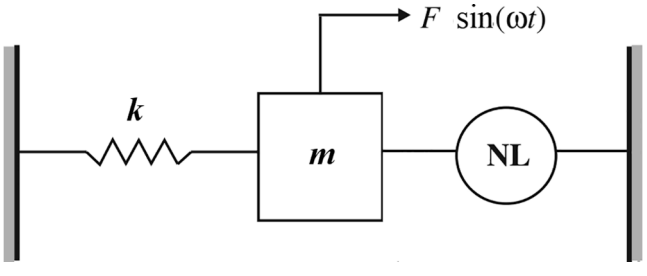

Fig. 1. SDOF system, $m = 1\text{kg}$, $k = 100\text{N/m}$, $F = 1\text{N}$,.$\omega = 9.85\text{rad/s}$.

results in a linear behaviour after the microslip stage as shown in Fig. 2a (left).

The effect of different $g_1(x)$ and $g_2(x)$ functions on the resultant Hysteresis loops is examined in Fig. 2. In Fig. 2b, three different functions for $g_1(x)$ and $g_2(x)$ are considered and their corresponding hysteresis loops for two cases explained in the following are shown in Fig. 2a. The two cases considered are $g_1(x) = g_2(x)$ (i.e., case I) and $g_2(x) = 0$ (i.e., case II). The hysteresis loops corresponding to the first case, i.e. when $g_1(x) = g_2(x)$, is shown in red in Fig. 2a. For this case, $g_1(x)$ and $g_2(x)$ take three different functions, i.e. linear, quadratic and bilinear functions, as given in Equations (3) to (5), respectively.

$$g_1(x) = g_2(x) = E_t x \tag{3}$$

$$g_1(x) = g_2(x) = E_t x + E_{t2} x|x| \tag{4}$$

$$g_1(x) = g_2(x) = \begin{cases} E_t x, & x > 0 \\ E_{t3} x, & x \le 0 \end{cases} \tag{5}$$

The parameters used in the simulations are given in Table 1. The hysteresis loops corresponding to this case reveal important characteristics of the original Valanis model. The hysteresis loop is symmetric when $g_1(x)$ and $g_2(x)$ are odd symmetric functions, as in the case of linear and quadratic functions. However, when $g_1(x)$ and $g_2(x)$ are non-symmetric functions as in the case of bilinear function, the hysteresis loop becomes non-symmetric. Moreover, the shape of the hysteresis loop reflects the type of $g_1(x)$ and $g_2(x)$ functions used. When $g_1(x)$ and $g_2(x)$ are linear functions, the hysteresis loop is a pure symmetric loop with a linear behaviour after the micro-slip stage. This type of hysteresis loop corresponds to an ideal contact interface during vibration where there is no variation in the contact interface parameters, i.e. contact area, interfacial pressure, etc.

In the case where $g_1(x)$ and $g_2(x)$ are quadratic functions, the hysteresis loop is still symmetric, but the behaviour is nonlinear after the micro-slip stage. This nonlinear behaviour could be the effect of the bolt shank stiffness on the hysteresis loops in a real bolted joint contact interface [39]. For the case of non-symmetric bilinear $g_1(x)$ and $g_2(x)$ functions, a drifted non-symmetric hysteresis loop occurs as shown in Fig. 2a (right). This can represent the behaviour of a contact interface when micro-vibro-impacts are developed in the interfacial area [40]. A second case where $g_2(x) - F_{nl} = 0$ is considered while $g_1(x)$ is assumed to be linear, quadratic or bilinear function, as described above in equations (3–5). This results in a simple equation governing the restoring force of the nonlinear element in Fig. 1 as,

$$\dot{F}_{nl} = E_0 \dot{x} \left(1 + \frac{\lambda}{E_0} sign(\dot{x}) (g_1(x) - F_{nl}) \right) \tag{6}$$

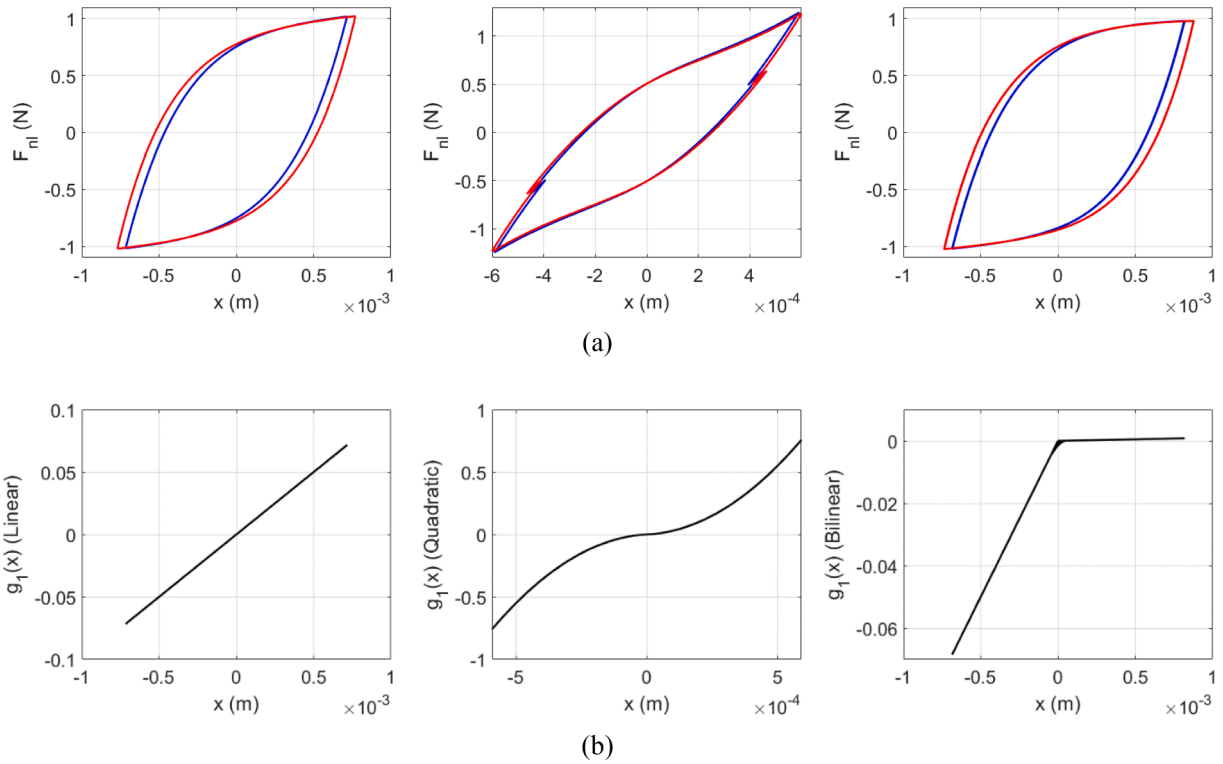

Fig. 2. The effect of different $g_1(x)$ and $g_2(x)$ functions on the hysteresis loops, (a) the hysteresis loops (case I in red line & case II in blue line) (b) corresponding $g_1(x)$ and $g_2(x)$ functions.

Table 1
Parameter values used in the simulations.

E_0	α_0	κ	E_t	E_{t2}	E_{t3}
3000	1	0.1	100	2×10^6	1

The hysteresis loops corresponding to this case are shown in blue in Fig. 2a. Comparing the red and blue hysteresis loops reveals that $g_2(x)$ has relatively negligible effects on the shape of the hysteresis loops. The results presented in Fig. 2a are obtained for a specific set of parameters. Further numerical investigations performed by the authors revealed that, at different sets of parameters values, the shape of the hysteresis loop remains the same when the case $g_2(x) - F_{nl} = 0$ is considered. It is worth mentioning that although the hysteresis shape remains unchanged, it is slightly scaled when $g_2(x) - F_{nl} = 0$ is considered. This will not affect the results since the focus in this study is on the shape of the hysteresis loop. This point is used as a guideline to introduce the generalized Valanis model in the next section.

2.2. The generalized Valanis model

The results presented in previous section showed that considering $g_2(x) - F_{nl} = 0$ in Equation (2) has negligible effects on the shape of the hysteresis loop. This leads to the following general form for the generalized Valanis model as,

$$\begin{cases} \dot{F}_{nl} = (C_1 + (P_1(x,\dot{x}) - C_2 F_{nl}))\dot{x}, & \dot{x} > 0 \\ \dot{F}_{nl} = (D_1 + (P_2(x,\dot{x}) - D_2 F_{nl}))\dot{x}, & \dot{x} \le 0 \end{cases} \tag{7}$$

where C_1, C_2, D_1 and D_2 are constant parameters. $P_1(x,\dot{x})$ and $P_2(x,\dot{x})$ can be identified using measured/simulated hysteresis loops. This is considered using numerical and simulated examples in the next sections. $P_1(x,\dot{x})$ and $P_2(x,\dot{x})$ functions can generate non-symmetric hysteresis loops, and this makes the simulation of the contact interface with variable normal pressure and variable contact area possible. It is worth mentioning that for a contact interface with constant parameters, i.e., constant normal pressure and constant contact area, a much simpler form of the new slip model can be considered. For such a system, the hysteresis loop is symmetric

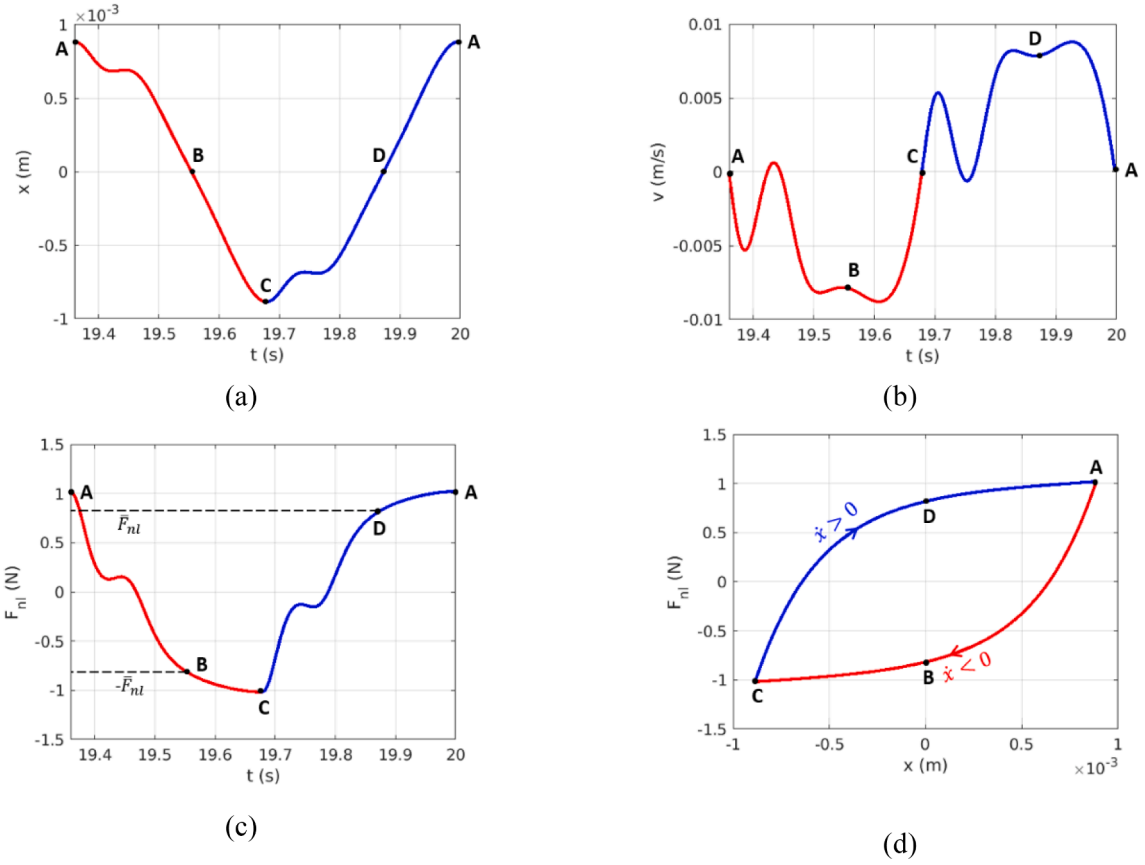

Fig. 3. (a) Displacement (b) velocity (c) friction force (d) hysteresis loop over one response cycle for $P(x,\dot{x}) = \alpha x$.

and the contact force can be obtained as,

$$\dot{F}_{nl} = \left(E_1 + \frac{\dot{x}}{|\dot{x}|}(P(x,\dot{x}) - E_2 F_{nl}) \right)\dot{x}, \tag{8}$$

where E_1 and E_2 are constant parameters. Solving Equations (7) and (8) results in closed form expressions for the hysteresis loops. For example, in Equation (8), if $P(x,\dot{x}) = \alpha x$ is considered, the expression representing the hysteresis loops is obtained as,

$$F_{nl}(x) = \frac{\dot{x}}{|\dot{x}|}\left[\left(\frac{E_1}{E_2} - \frac{\alpha}{{E_2}^2} \right) + ce^{-\frac{\dot{x}}{|\dot{x}|}E_2 x} \right] + \frac{\alpha}{E_2}x \tag{9}$$

where c is the constant of integration and can be evaluated using a single data set on the hysteresis loop. Point B or D in Fig. 3 is the best choice for calculating c. Points A and C can't be used for this purpose because at these points, $\dot{x} = 0$. Substituting the coordinates of point B or D into equation (9) gives,

$$c = \overline{F}_{nl} + \frac{\alpha}{{E_2}^2} - \frac{E_1}{E_2} \tag{10}$$

As another example, considering $P(x,\dot{x}) = \alpha x + \beta x^2|\dot{x}|$ results in the following expression for the hysteresis loops,

$$F_{nl}(x) = \frac{\dot{x}}{|\dot{x}|}\left(\frac{E_1{E_2}^2 - \alpha E_2 + 2\beta}{{E_2}^3} + \frac{\beta}{E_2}x^2 + ce^{-\frac{\dot{x}}{|\dot{x}|}E_2 x} \right) - \frac{2\beta - E_2\alpha}{{E_2}^2}x \tag{11}$$

The constant of integration in this case is obtained as,

$$c = \overline{F}_{nl} - \frac{E_1{E_2}^2 - \alpha E_2 + 2\beta}{{E_2}^3} \tag{12}$$

In the next section, an identification method is introduced for $P(x,\dot{x})$ by using measured/simulated hysteresis loops.

2.3. Identification of $\boldsymbol{P(x,\dot{x})}$ in the generalized Valanis model

Consider that a measured/simulated hysteresis loop, i.e. the set of points $[x_i \& F_{nli}]$, is known. x_i and F_{nli} are respectively the displacement and friction force at time instant t_i. The aim of this section is to identify $P(x,\dot{x})$ by using the measured hysteresis loop.

Equation (8) can be written as,

$$\frac{dF_{nl}}{dx} = E_1 + \frac{\dot{x}}{|\dot{x}|}(P(x,\dot{x}) - E_2 F_{nl}), \tag{13}$$

where $\frac{dF_{nl}}{dx}$ can be obtained using numerical differentiation. Knowing x_i, F_{nli} and $\left(\frac{dF_{nl}}{dx}\right)_i$ at each time instant t_i, the unknown parameters E_1 and E_2 and $P(x,\dot{x})$ can be identified using optimization algorithms. Polynomials are suitable choice for $P(x,\dot{x})$. Using a modified Pascal's triangle given in the Appendix 7.1, the following general form can be considered,

$$P(x,\dot{x}) = a_1 x + a_2\dot{x} + a_3 x^2 + a_4 x\dot{x} + a_5\dot{x}^2 + \cdots \tag{14}$$

The order of polynomials considered in Equation (14) depends upon the level of complexity of the hysteresis loop. Substituting Equation (14) into Equation (13) and considering the branch of the hysteresis loop corresponding to $\dot{x} > 0$, the unknown parameters can be identified as follows,

$$\begin{bmatrix} 1 & x_1 & \dot{x}_1 & x_1^2 & x_1\dot{x}_1 & \dot{x}_1^2 & -(F_{nl})_1 \\ 1 & x_2 & \dot{x}_2 & x_2^2 & x_2\dot{x}_2 & \dot{x}_2^2 & -(F_{nl})_2 \\ \vdots & \vdots & \vdots & \vdots & \vdots & \vdots & \vdots \\ 1 & x_q & \dot{x}_q & x_q^2 & x_q\dot{x}_q & \dot{x}_q^2 & -(F_{nl})_q \end{bmatrix} \begin{Bmatrix} E_1 \\ a_1 \\ a_2 \\ a_3 \\ a_4 \\ a_5 \\ E_2 \end{Bmatrix} = \begin{Bmatrix} \left(\frac{dF_{nl}}{dx}\right)_1 \\ \left(\frac{dF_{nl}}{dx}\right)_2 \\ \vdots \\ \left(\frac{dF_{nl}}{dx}\right)_q \end{Bmatrix} \tag{15}$$

Re-writing Equation (15) in a matrix form gives,

$$[\boldsymbol{H}]\{\boldsymbol{d}\} = \{\boldsymbol{b}\} \tag{16}$$

The vector of unknown parameters $\{\boldsymbol{d}\}$ can be calculated using a least square procedure as,

$$\{\boldsymbol{d}\} = \left([\boldsymbol{H}]^T[\boldsymbol{H}]\right)^{-1}\{\boldsymbol{b}\} \tag{17}$$

It should be noted that if the system of equations defined by Equation (16) are ill-conditioned, regularization techniques may be

used to overcome the ill-posed condition [41,42]. It is worth mentioning that in the above analysis, only one branch of the hysteresis loop was used to identify the model parameters (i.e. the branch corresponding to $\dot{x} > 0$). The next section considers numerical examples to verify the applicability of the proposed identification approach.

3. Verification of the identification approach

In this section the accuracy of the identification method introduced in the previous sections is examined by using numerical examples. Four examples are considered in this section. Different functions are considered for $P(x,\dot{x})$ and the hysteresis loops are simulated. Then, by using the hysteresis loops and the method proposed in previous section, $P(x,\dot{x})$ is identified and reconstructed.

3.1. Example 1: $\boldsymbol{P(x,\dot{x}) = \alpha x}$

Equation (8) shows the equations governing the friction force in this example, for particular parameter values,

$$\dot{F}_{nl} = \left(10 + \frac{\dot{x}}{|\dot{x}|}(5x - 20F_{nl})\right)\dot{x}, \tag{18}$$

Solving the set of Equations (1) and (18) simultaneously, the hysteresis loop is obtained using the steady state part of the response as is shown in Fig. 4. With F_{nl} known, $\frac{dF_{nl}}{dx}$ is calculated and substituted into Equation (15) for parameter identification. The identified parameters are reported in Table 2. The simulation results corresponding to one branch of the hysteresis loop are considered in the identification. Equivalent results are obtained if the other branch is used.

It is worth mentioning that $\frac{dF_{nl}}{dx}$ fluctuates over a short interval at the two extreme ends of the x range. These intervals are not considered in the identification of the unknown parameters.

3.2. Example 2: $\boldsymbol{P(x,\dot{x}) = \alpha x + \beta x^2|\dot{x}|}$

Fig. 5 shows the results for simulated, identified and analytical hysteresis loops when.

$\dot{F}_{nl} = (10 + \frac{\dot{x}}{|\dot{x}|}(30x + 1400x^2|\dot{x}| - 20F_{nl}))\dot{x}$ is considered. The exact and identified parameters are tabulated in Table 3. The results show that the proposed method identified the model parameters with a high accuracy. As the branch of the hysteresis loop corresponding to.

$\dot{x} > 0$ is used in the identification, the following $[\boldsymbol{H}]$ matrix is used in the identification procedure for this example,

$$[\boldsymbol{H}] = \begin{bmatrix} 1 & x_1 & x_1^2\dot{x}_1 & -(F_{nl})_1 \\ 1 & x_2 & x_2^2\dot{x}_2 & -(F_{nl})_2 \\ \vdots & \vdots & \vdots & \vdots \\ 1 & x_q & x_q^2\dot{x}_q & -(F_{nl})_q \end{bmatrix} \tag{19}$$

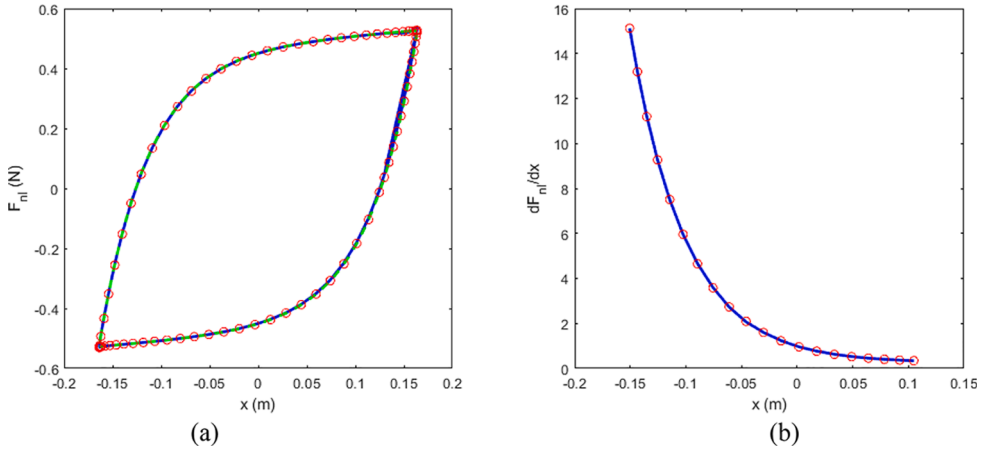

Fig. 4. (a) Hysteresis loop (b) $\frac{dF_{nl}}{dx}$ simulated (solid blue), reconstructed (red circles) and closed form solution (i.e. Eq. (9)) (dashed green).

Table 2
Exact and identified parameters ($P(x,\dot{x}) = \alpha x$).

	E_1	α	E_2
Exact	10	5	20
Identified	10.004	5.017	20.011

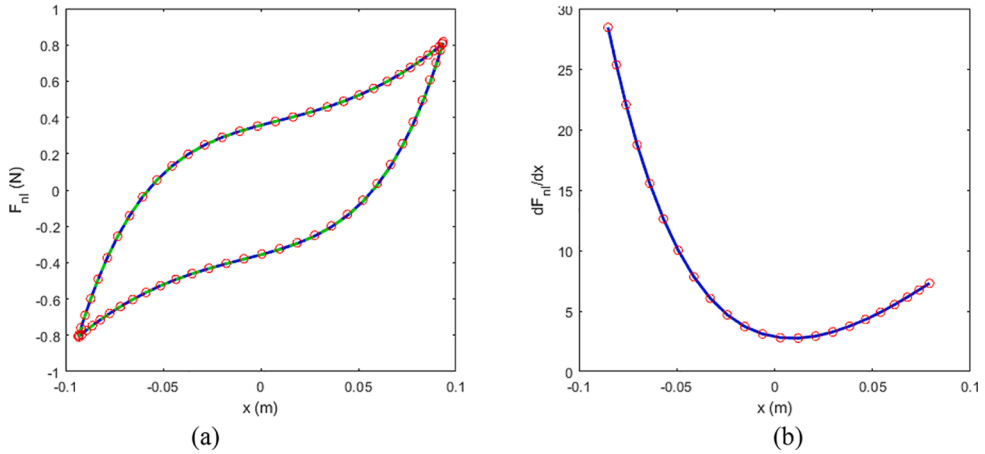

Fig. 5. (a) Hysteresis loop (b) $\frac{dF_{nl}}{dx}$ simulated (solid blue), reconstructed (red circles) and closed form solution (i.e. Eq. (10)) (dashed green).

Table 3
Exact and identified parameters ($P(x,\dot{x}) = \alpha x + \beta x^2|\dot{x}|$).

	E_1	α	β	E_2
Exact	10	30	1400	20
Identified	10.018	30.53	1397.1	20.042

3.3. *Example 3:* $P(x,\dot{x}) = \alpha x + \beta e^x \dot{x}$

In the previous two examples, the exact form of $P(x,\dot{x})$ was considered in the identification procedure. However, this is not the case when the hysteresis loop is obtained by measurement or via numerical simulation, as described in the next sections. In such circumstances, the identification approach introduced in Section 2.3 must be used with a polynomial function considered for $P(x,\dot{x})$. In this section, $\dot{F}_{nl} = (30 + \frac{\dot{x}}{|\dot{x}|}[(5x + 3e^x\dot{x}) \times 10^4 - 500F_{nl}])\dot{x}$ is used to simulate the hysteresis loop shown in Fig. 6. Then, in the identification procedure, the following polynomial is considered,

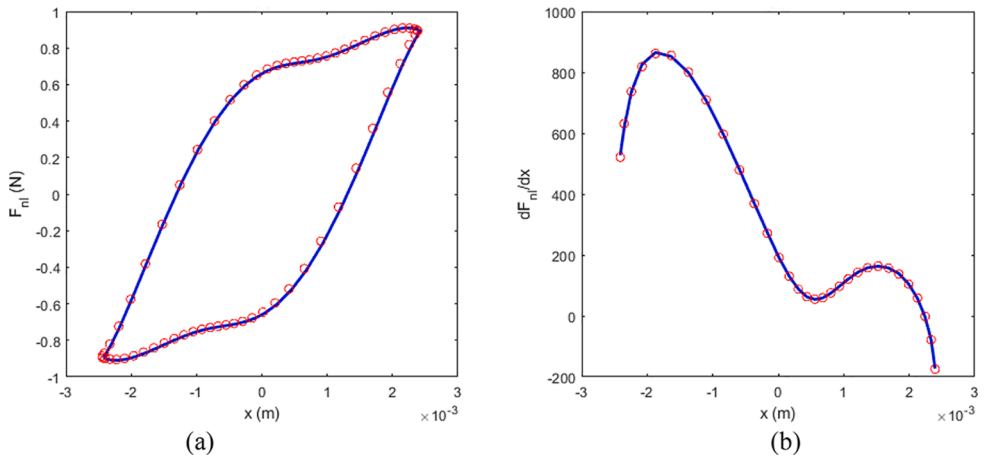

Fig. 6. (a) Hysteresis loop (b) $\frac{dF_{nl}}{dx}$ simulated (solid blue) and reconstructed (red circles).

$$P(x,\dot{x}) = a_1 x + a_2 \dot{x} + a_3 x\dot{x} \tag{20}$$

The identified parameters a_1, a_2 and a_3 are reported in Table 4.

The results presented in Fig. 6 indicate that the identification method introduced in the previous section identifies the hysteresis loops with an acceptable accuracy.

3.4. Example 4: $\boldsymbol{P}(\boldsymbol{x},\dot{\boldsymbol{x}}) = \begin{cases} \boldsymbol{\alpha_1 sin(x)}, & \dot{\boldsymbol{x}} \geq 0 \\ \boldsymbol{\alpha_2 x}, & \dot{\boldsymbol{x}} < 0 \end{cases}$

The functions used in this example are $\dot{F}_{nl} = (10 + (40\sin x - 20F_{nl}))\dot{x}, \dot{x} \geq 0$ and $\dot{F}_{nl} = (10 - (15x - 20F_{nl}))\dot{x}, \dot{x} < 0$. The following assumed functions are used in the identification procedure.

$$P(x,\dot{x}) = \begin{cases} a_1 x + a_2 x^3 + a_3 x^5, & \dot{x} \geq 0 \\ a_4 x, & \dot{x} < 0 \end{cases} \tag{21}$$

Fig. 7 shows the simulated and reconstructed results and in Table 5 the parameters of the functions used in the identification are reported.

The results presented in this section show that the method proposed in the previous section is effective in the generalized Valanis model parameter identification. The next section considers the use of the generalized Valanis model and the identification approach in modelling a bolted flange structure.

4. Bolted joint flange structure

4.1. FE modelling and response simulation

The 3D detailed finite element model simulating the micro-slip mechanism of a bolted flange by Jamia et al. [43] is used in this study. Two L-shaped flanges connected via 3 identical M8 bolts are considered, and the geometric details are shown in Fig. 8. The commercial software ANSYS Workbench was used to perform the finite element analysis. A fine mesh was adopted in the contact interface of the joint, bolts, nuts and washers as shown in Fig. 9a. Moreover, a fine mesh was considered near the flange holes to accurately capture the micro slip behaviour at the contact surfaces.

The contact types between different elements of the system were assigned using the embedded contact elements in Ansys (i.e., bonded, frictionless and frictional) and the penalty-based contact algorithms (i.e., Augmented Lagrange and Pure Penalty) are considered to calculate the nonlinear solutions in the contact surfaces. Regarding boundary conditions, the lower side of the bottom flange was constrained. Furthermore, a preload was applied to the shank of each bolt. The load case shown in Fig. 9 is considered where two equal forces with opposite directions were applied in the transverse direction of the contact interface between the two flanges to excite the sliding behaviour in the contact surfaces.

A dynamic analysis was performed where the system was subjected to a harmonic force defined as $F_1(t) = F_2(t) = |F|\sin(\omega t)$ where $|F| = 4$ kN. A time integration simulation was performed over a period of 4 s using a time step of 0.0025 s. At each time step, the relative displacement of a point from the contact surfaces was calculated. Four different excitation frequencies were considered. The relative displacement in the x-direction was collected in order to calculate and plot the simulated hysteresis loops considered in the next sections. More details about this FE model can be found in Jamia et al. [43].

4.2. Mathematical modelling

In this section a mathematical model is used to describe the dynamic response of the bolted-flange joint structure by using Euler-Bernoulli beam theory as represented in Fig. 10,

The equations governing the structure are derived as,

$$EIw_1^{''''} + \rho A\ddot{w}_1 = (F\sin\omega t - N(t))\delta\left(x - \frac{L}{2}\right), \quad 0 < x < L/2 \tag{22}$$

$$EIw_2^{''''} + \rho A\ddot{w}_2 = (N(t) - F\sin\omega t)\delta\left(x - \frac{L}{2}\right), \quad L/2 < x < L \tag{23}$$

where w_1 and w_2 are the lateral displacements in beams 1 and 2, F is the amplitude of the external forces applied to the structure at the joint section. $N(t)$ shows the nonlinear part of the contact force in the tangential direction (i.e. y direction) at the interfacial area.

Table 4
Identified parameters for Equation (20).

E_1	a_1	a_2	a_3	E_2
29.52	5×10^4	29991	22104	499.53

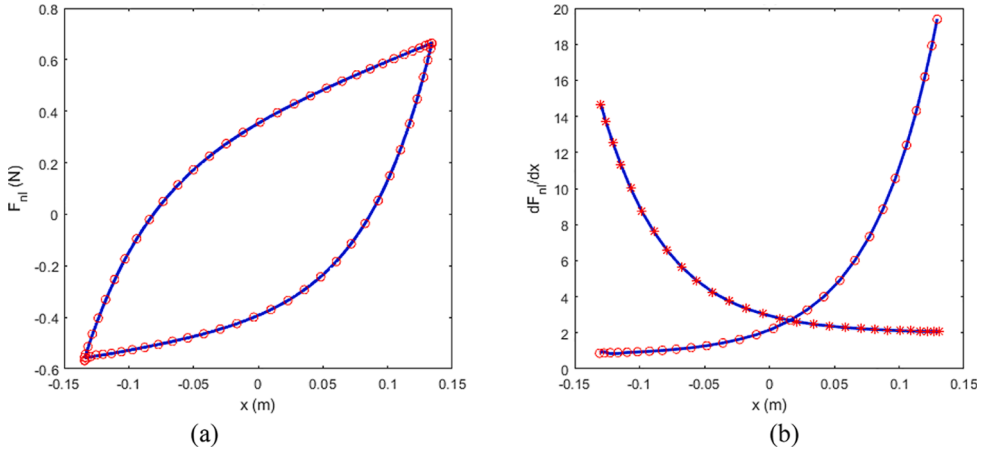

Fig. 7. (a) Hysteresis loop (b) $\frac{dF_{nl}}{dx}$ simulated (solid blue), reconstructed for $\dot{x} < 0$ (red circles) and reconstructed for $\dot{x} \geq 0$ (red stars).

Table 5
Identified parameters for Equation (21).

E_1	a_1	a_2	a_3	a_4	E_2
10	40.09	−22.24	1176.6	15.14	20.02

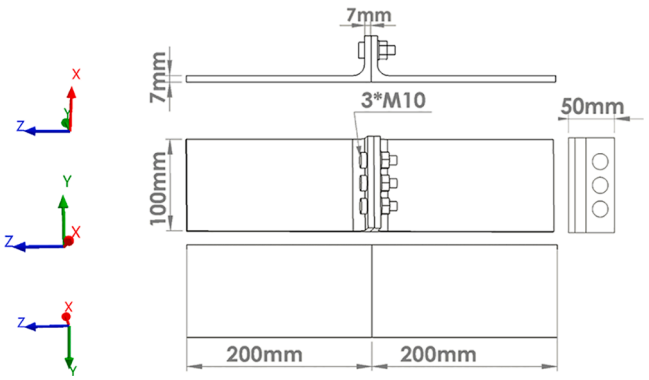

Fig. 8. Bolted flange geometry and dimensions (mm) (From Jamia et al. [43]).

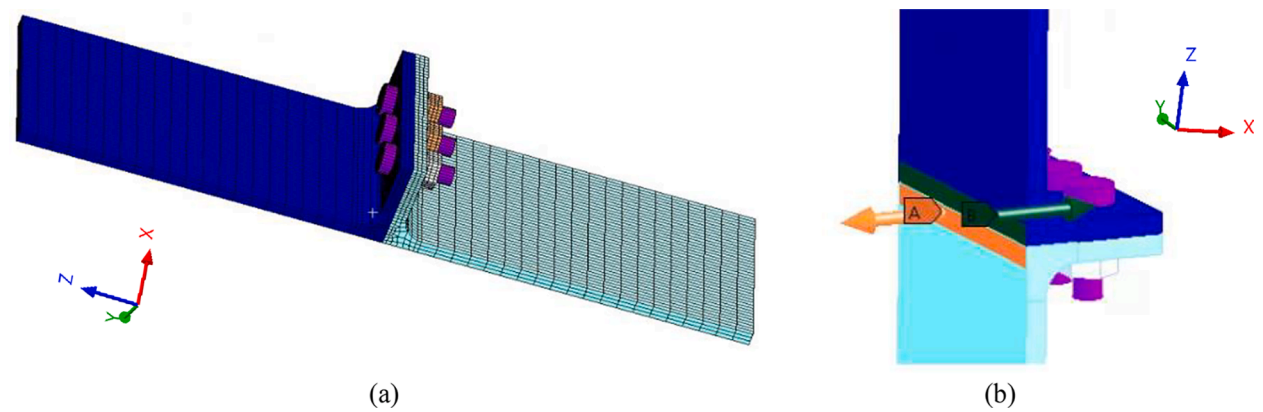

Fig. 9. (a) Two bolted flanges model (b) External loads.

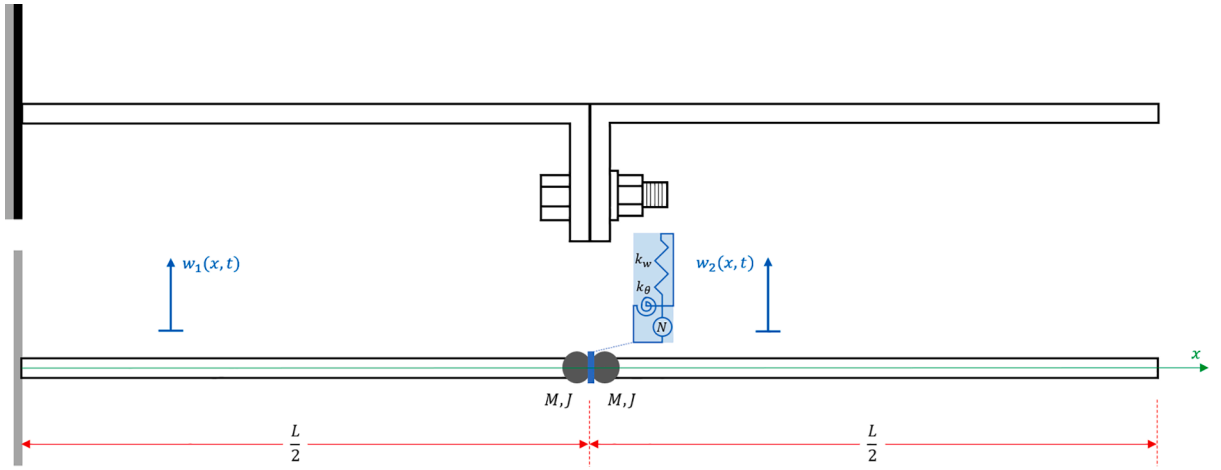

Fig. 10. The mathematical model for the bolted-joint flange structure.

The equivalent linear effect of the contact interface in the tangential and normal directions are shown by lateral and torsional springs, i.e. k_w and k_θ, in Fig. 10, respectively. M and J are the mass effects of the flange sections on the bending behaviour of the main parts of the structure. The governing equations are subjected to the following boundary conditions,

$$w_1(0,t) = w_1'(0,t) = w_2''(L,t) = w_2'''(L,t) = 0 \tag{24-27}$$

The compatibility requirements at $x = L/2$ are,

$$EIw_1''' = M_1\ddot{w}_1 - k_w(w_2 - w_1) \tag{28}$$

$$EIw_1'' = -J_1\ddot{w}_1' + k_\theta\left(w_2' - w_1'\right) \tag{29}$$

$$EIw_2''' = -M_2\ddot{w}_2 - k_w(w_2 - w_1) \tag{30}$$

$$EIw_2'' = J_2\ddot{w}_2' + k_\theta\left(w_2' - w_1'\right) \tag{31}$$

In this study it is considered that k_θ is constant. k_w depends on the shape of the hysteresis loop (i.e. either symmetric or non-symmetric) and is obtained following the approach described in Fig. 9 or the identification technique described in Section 2.3.

$N(t)$ in the equations (22) and (23) is defined based on Equation (7) as,

$$\dot{N}(t) = \left(\bar{k}_w + \frac{\dot{z}}{|\dot{z}|}\left(\bar{P}(z,\dot{z}) - \bar{k}N(t)\right)\right)\dot{z}, \tag{32}$$

where $z(t)$ is the relative displacement in the contact interface defined as,

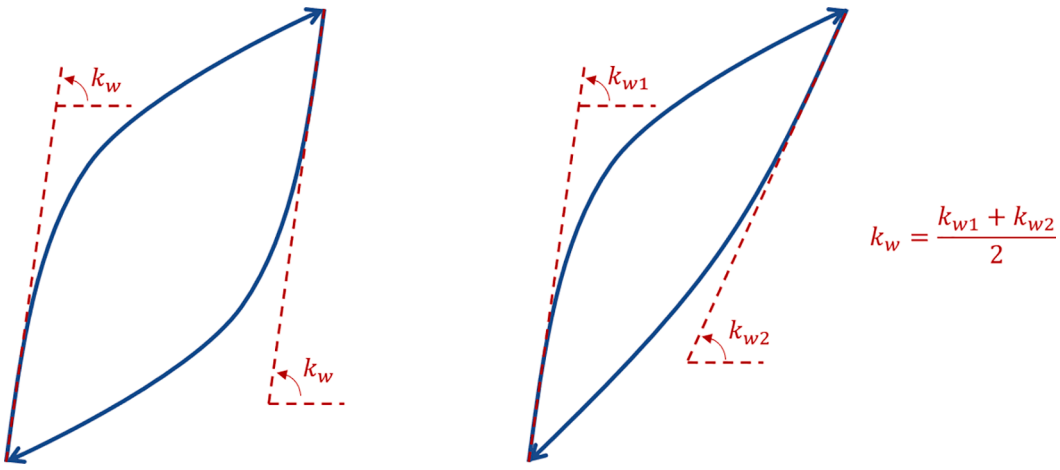

Fig. 11. Approach to determine k_w by using the hysteresis loop.

$$z(t) = w_1\left(\frac{L}{2}, t\right) - w_2\left(\frac{L}{2}, t\right) \tag{33}$$

$\bar{k}_w$, $\bar{P}$ and $\bar{k}$ can be different for hysteresis loop branches corresponding to $\dot{z} > 0$ and $\dot{z} < 0$ as described in the previous section. Based on the approach described in Fig. 11, for the case of a symmetric hysteresis loop, $\bar{k}_w = k_w$. For a non-symmetric hysteresis loop, $\bar{k}_w = k_{w1}$ for the branch corresponding to $\dot{z} > 0$ and $\bar{k}_w = k_{w2}$ for the branch corresponding to $\dot{z} < 0$.

4.3. Dynamic response analysis

In the dynamic response analysis considered for the structure shown in Fig. 12, linear mode shapes are needed. Therefore, linear modal analysis is considered for equations (22) and (23) by removing the external excitation and neglecting the non-linear forces from these equations, i.e. by setting $N(t) = F = 0$. The results for the linear modal analysis and parameter identification are provided in the next sections.

The assumed mode method is used to solve the governing Equations (22) and (23). The solution is approximated by using the first mode shape as,

$$w_1(x,t) = Y_{11}(x)q(t), \qquad 0 < x < \frac{L}{2} \tag{34}$$

$$w_2(x,t) = Y_{12}(x)q(t), \qquad \frac{L}{2} < x < L \tag{35}$$

where $Y_{11}(x)$ and $Y_{12}(x)$ form the first mode shape $Y_1(x)$ and are obtained by solving the linear problem given in the Appendix 7.2.

Substituting Equations (34) and (35) into equations (22) and (23), multiplying both sides by $Y_1(x)$ and integrating over the structure length, i.e. $x = [0, L]$, results into the following set of nonlinear equations,

$$b_1\ddot{q}(t) + b_2 q(t) = \sin\omega t - N(t) \tag{36}$$

$$\dot{N}(t) = \left(k_w + \frac{\dot{q}(t)}{|\dot{q}(t)|}\left(P(\eta,\dot{\eta}) - k_n N(t)\right)\right)\dot{\eta} \tag{37}$$

where,

$$b_1 = \rho A\left[\int_0^{L/2} {Y_{11}}^2 dx + \int_{L/2}^{L} {Y_{12}}^2 dx\right] \Big/ b_3 \tag{38}$$

$$b_2 = EI\left[\int_0^{L/2} Y_{11}{Y_{11}}'''' dx + \int_{L/2}^{L} Y_{12}{Y_{12}}'''' dx\right] \Big/ b_3 \tag{39}$$

$$b_3 = \left[Y_{11}\left(\frac{L}{2}\right) - Y_{12}\left(\frac{L}{2}\right)\right] \tag{40}$$

$$\eta(t) = b_3 q(t) \tag{41}$$

By solving Equations (36) and (37), the dynamic response is obtained.

5. Results and discussion

In this section the suitability of the new slip model proposed in the previous sections in predicting the dynamic response of bolted flange structures is discussed and the results are presented. Four hysteresis loops simulated by the FE model of Section 4.1 are used in this section. The procedure employed is as follows: First, the method described in Section 2.3 is used to identify the equations governing the simulated hysteresis loops. Then the slip model for the contact interface is characterized by using one of the simulated hysteresis loops. This results in the identification of k_w. k_w can equivalently be estimated by using the approach described in Fig. 12. By estimating k_w, the linear part of Equations (22) and (23) are solved for the natural frequencies as described in the Appendix 7.2. Then, the unknown linear parameters in the mathematical model shown in Fig. 12, i.e. k_θ, M and J, are identified by comparing experimental and analytical natural frequencies using an eigen-sensitivity based approach [44]. A numerical/FE model can also assist in the linear model parameter identification. Finally, the first mode shape and the identified slip model are substituted into equations (36)-(41) and the hysteresis loops are reconstructed by solving these equations and are compared with the initial simulated ones. The next section considers identification of the generalized Valanis model using one of the simulated hysteresis loops.

5.1. Generalized Valanis model identification

The simulated hysteresis loops used in this paper are shown in Fig. 12. One hysteresis loop, i.e. Fig. 12(b), is used to identify the

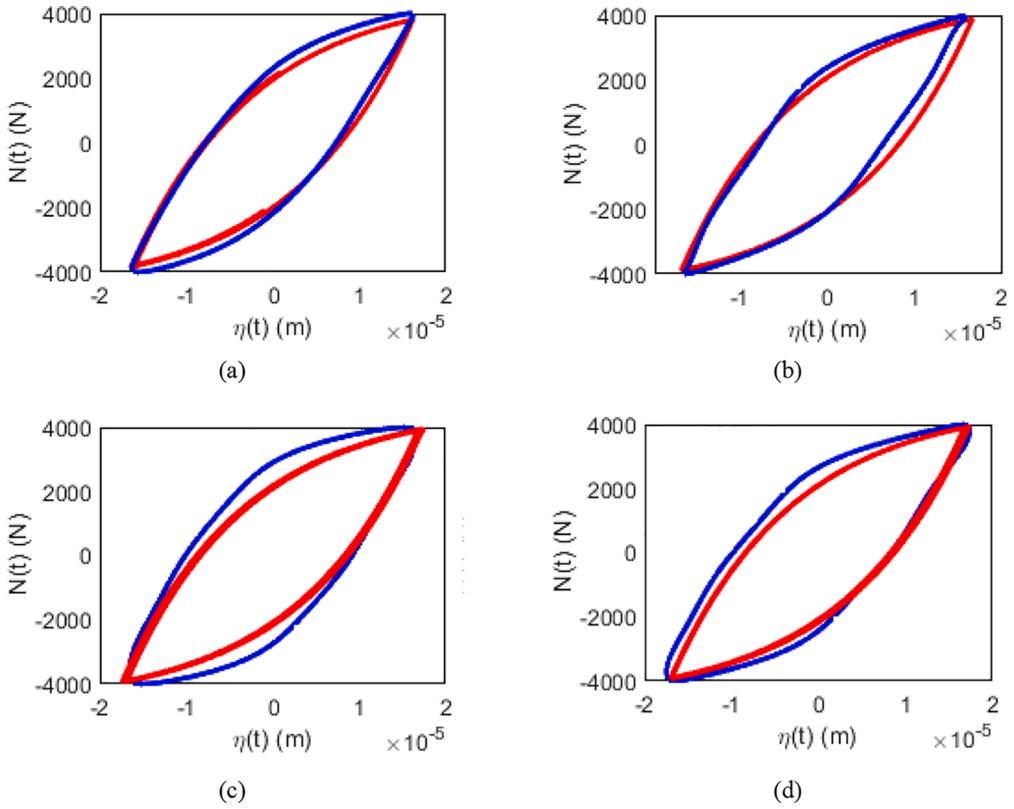

Fig. 12. Simulated (blue) and reconstructed (red) hysteresis loops at different excitation frequencies (a) $\omega = 7$Hz (b) $\omega = 15$Hz (c) $\omega = 20$Hz (d).$\omega = 25$Hz

generalized Valanis model parameters. Equation (37) is considered to govern this hysteresis loop. The polynomial $P(\eta, \dot{\eta})$ given in Equation (42) is considered. Using the method proposed in Section 2.3, the different parameters of the polynomial P are identified and reported in Table 6 for the branch of hysteresis loop corresponding to $\dot{\eta} > 0$,

$$P(\eta, \dot{\eta}) = a_1\eta + a_2\dot{\eta} + a_3\dot{\eta}^2 + a_4\dot{\eta}^3 \tag{43}$$

The identified parameter k_w can equivalently be estimated by using the approach described in Fig. 11.

5.2. Linear parameter identification

The simulated natural frequencies reported in Table 8 are used in this section to construct a base linear system for the flange structure, to be used in the nonlinear response analysis in the next section. The linear parameters in the mathematical model described in Fig. 10 are k_w, k_t, M and J from which k_w was identified in the previous section. The remaining linear parameters are estimated in this section using three natural frequencies and adopting an eigen-sensitivity based identification approach. The identified parameters and the comparison between simulated and identified natural frequencies are reported in Tables 7 and 8. Table 8 shows that the identified model can effectively predict the flange structure dynamics up to its third mode. The predicted natural frequencies by the model proposed in this paper shows a higher accuracy compared to the model used in [43].

The next section considers nonlinear dynamic analysis by using the linear base model identified in this section.

5.3. Non-linear dynamic analysis

The linear base model and the generalized Valanis model identified in the previous sections are used and Equations (36) and (37) are solved for the nonlinear dynamic response simulation of the flange structure. The simulated dynamic responses are used to

Table 6
Identified parameters for the generalized Valanis model.

$k_w(N/m)$	a_1	a_2	a_3	a_4	k_n
3.33×10^8	-2175.3	2.70×10^5	273.2	0.314	7.13×10^4

Table 7
Identified linear parameters for the contact model.

k_t(kNm/rad)	M(g)	J(kg.m^2)
22.089	69.12	16.011×10^{-5}

Table 8
Natural frequency comparison (Hz).

	ω_1	ω_2	ω_3
Simulated	34.93	196.84	589.97
Identified	34.60	197.2	590.08
Error (%)	−0.94	0.18	0.02

reconstruct the hysteresis loops. A comparison between the original and reconstructed hysteresis loops are shown in Fig. 12. It is worth mentioning that in the results shown in Fig. 12, the slip model identified by using one hysteresis loop, i.e. @ $\omega = 15Hz$, is used to reconstruct the other hysteresis loops. The results shown in Fig. 12 indicate the effectiveness and predictability of the generalized Valanis model proposed in this paper.

6. Conclusions

A generalized Valanis model has been proposed for the hysteretic behaviour of frictional contact interfaces which can be used to generate both symmetric and non-symmetric hysteresis loops. The formulation proposed makes identification of model parameters possible by using measured/simulated results. Different numerical examples were used to show the effectiveness of proposed identification approach. To demonstrate the integration of the new model into a simplified dynamic model of an assembled structure, simulation results of a bolted flange structure were used. The identification results presented show that the proposed slip model can be used effectively to simulate the behaviour of frictional contact interfaces in assembled structures.

Declaration of Competing Interest

The authors declare that they have no known competing financial interests or personal relationships that could have appeared to influence the work reported in this paper.

Acknowledgements

The authors gratefully acknowledge the support of the Engineering and Physical Sciences Research Council through the award of the Programme Grant “Digital Twins for Improved Dynamic Design”, grant number EP/R006768/1.

Appendix

A.1. Modified Pascal triangle

$$\begin{array}{ccccc} & & 1 & & \\ & & x & \dot{x} & \\ & x^2 & x\dot{x} & \dot{x}^2 & \\ x^3 & x^2\dot{x} & x\dot{x}^2 & \dot{x}^3 & \end{array}$$

A.2. Linear modal analysis

The equations governing the linear behaviour of flange structure are derived as,

$$EIw_1^{''''} + \rho A\ddot{w}_1 = 0, \quad 0 < x < L/2 \tag{A1}$$

$$EIw_2^{''''} + \rho A\ddot{w}_2 = 0, \quad L/2 < x < L \tag{A2}$$

The boundary conditions and compatibility requirements are defined in Equations (16)-(24). By considering a harmonic response as $w_1(x,t) = Y_1(x)\sin\omega_n t$ and $w_2(x,t) = Y_2(x)\sin\omega_n t$ and substituting into the governing equations, boundary conditions and compatibility requirements one obtains the following equations,

$$Y_1''''+\lambda^4 Y_1=0,\qquad Y_2''''+\lambda^4 Y_2=0,\qquad \lambda^4=\frac{\rho A}{EI}\omega_n^2 \tag{A3-A4}$$

$$Y_1(0)=Y_1'(0)=Y_2''(L)=Y\prime\prime_2'(L)=0, \tag{A5-A8}$$

$$EIY_1'''+k_w(Y_2-Y_1)+\omega_n^2 M_1 Y_1=0,\quad @x=L/2 \tag{A9}$$

$$EIY_1''-k_\theta\left(Y_2'-Y_1'\right)-\omega_n^2 J_1 Y_1'=0,\quad @x=L/2 \tag{A10}$$

$$EIY_2'''+k_w(Y_2-Y_1)-\omega_n^2 M_2 Y_2=0,\quad @x=L/2 \tag{A11}$$

$$EIY_2''-k_\theta\left(Y_2'-Y_1'\right)+\omega_n^2 J_2 Y_2'=0,\quad @x=L/2 \tag{A12}$$

Solving equations (A3) and (A4) results in the following solutions,

$$Y_1(x)=[\boldsymbol{Q}(\boldsymbol{x})]\{\boldsymbol{c}_1\},\quad 0<x<L/2 \tag{A13}$$

$$Y_2(x)=[\boldsymbol{Q}(\boldsymbol{x})]\{\boldsymbol{c}_2\},\quad L/2<x<L \tag{A14}$$

where,

$$[\boldsymbol{Q}(\boldsymbol{x})]=[\,sin(\lambda x)\quad cos(\lambda x)\quad sinh(\lambda x)\quad cosh(\lambda x)\,] \tag{A15}$$

$$\{\boldsymbol{c}_1\}=[\,c_{11}\quad c_{12}\quad c_{13}\quad c_{14}\,]^T \tag{A16}$$

$$\{\boldsymbol{c}_2\}=[\,c_{21}\quad c_{22}\quad c_{23}\quad c_{24}\,]^T \tag{A17}$$

Substituting Equations (A13) and (A14) into Equations (A5-A12) one may obtain,

$$[\Gamma]\{c\}=\begin{bmatrix} Q(0) & 0\\ Q'(0) & 0\\ 0 & Q''(L)\\ 0 & Q'''(L)\\ EIQ'''\left(\frac{L}{2}\right)+\left(\omega_n^2M_1-k_w\right)Q\left(\frac{L}{2}\right) & k_wQ\left(\frac{L}{2}\right)\\ EIQ''\left(\frac{L}{2}\right)+\left(k_\theta-\omega_n^2J_1\right)Q'\left(\frac{L}{2}\right) & -k_\theta Q'\left(\frac{L}{2}\right)\\ -k_wQ\left(\frac{L}{2}\right) & EIQ'''\left(\frac{L}{2}\right)+\left(k_w-\omega_n^2M_1\right)Q\left(\frac{L}{2}\right)\\ k_\theta Q'\left(\frac{L}{2}\right) & EIQ''\left(\frac{L}{2}\right)+\left(\omega_n^2J_1-k_\theta\right)Q'\left(\frac{L}{2}\right) \end{bmatrix}\begin{Bmatrix}\{c_1\}\\ \{c_2\}\end{Bmatrix}=\{0\} \tag{A18}$$

where $(\,)'=\frac{d(\,)}{dx}$..

The natural frequencies are obtained by solving $|\Gamma|=0$. By substituting the natural frequencies in Equation (A18), the mode shapes are known.

References

[1] R. Bouc, Forced vibration of mechanical systems with hysteresis. Proceedings of the fourth conference on non-linear oscillation, Prague, 1967.
[2] R. Bouc, A mathematical model for hysteresis, Acustica 21 (1971) 16–25.
[3] Y.K. Wen, Method for random vibration of hysteretic systems, J. Eng. Mech. 102 (1976) 246–263.
[4] M. Ismail, F. Ikhouane, J. Rodellar, The hysteresis Bouc-Wen model, a survey, Arch. Comput. Methods Eng. 16 (2009) 161–188.
[5] Y.Q. Ni, J.M. Ko, C.W. Wong, Identification of non-linear hysteretic isolators from periodic vibration tests, J. Sound Vib. 217 (4) (1998) 737–756.
[6] M. Oldfield, H. Ouyang, J.E. Mottershead, Simplified models of bolted joints under harmonic loading, Comput. Struct. 84 (1–2) (2005) 25–33.
[7] T. Sireteanu, M. Gluclea, A.M. Mitu, Identification of an extended Bouc-Wen model with application to seismic protection through hysteretic devices, Comput. Mech. 45 (5) (2010) 431–441.
[8] X. Zhu, X. Lu, Parametric identification of Bouc-Wen model and its application in mild steel damper modeling, Procedia Eng. 14 (2011) 318–324.
[9] M.A. Zaman, U. Sikder, Bouc-Wen hysteresis model identification using Modified Firefly algorithm, J. Magn. Magn. Mater. 395 (2015) 229–233.
[10] G.A. Ortiz, D.A. Alvarex, D. Bedoya-Ruiz, Identification of Bouc-Wen type models using the transitional Markov chain Monte Carlo method, Comput. Struct. 146 (2015) 252–269.
[11] J.P. Noel, A.F. Esfahani, G. Kerschen, J. Schoukens, A nonlinear state-space approach to hysteresis identification, Mech. Syst. Sig. Process. 84 (Part B) (2017) 171–184.

[12] A.T. Mathis, N.N. Balaji, R.J. Kuether, A.R. Brink, M.R.W. Brake, D.D. Quinn, A Review of Damping Models for Structures with Mechanical Joints, Appl. Mech. Rev. 72 (4) (2020).
[13] C.W. Wong, Y.Q. Ni, J. Ko, M., Steady-state oscillation of hysteretic differential model. II: Performance analysis, J. Eng. Mech. 120 (11) (1994) 2299–2325.
[14] Dahl P. R., A solid friction model, Technical report, The Aerospace corportation, El Segundo, California, (1968).
[15] P.R. Dahl, Solid friction damping of mechanical vibrations, AIAA J. 14 (1996) 1675–1682.
[16] C.C. De-Wit, H. Olsson, K.J. Åström, P. Lischinsky, A new model for control of systems with friction, IEEE Trans. Autom. Control 40 (1995) 419–425.
[17] Olsson, H., Control systems with friction, Doctoral dissertation, (1996), Lund University.
[18] H. Olsson, K.J. Åström, C.C. de Wit, M. Gäfvert, P. Lischinsky, Friction models and friction compensation, Eur. J. Control 3 (1998) 176–195.
[19] N.B. Do, A.A. Ferri, O.A. Bauchau, Efficient Simulation of a Dynamic System with LuGre Friction, J. Comput. Nonlinear Dyn. 2 (2007) 281–289.
[20] K.J. Åström, C.C. De-Wit, Revisiting the LuGre Friction Model, IEEE Control Syst. 28 (6) (2008) 101–114.
[21] J. Koopman, D. Jeltsema, M. Verhaegen, Port-Hamiltonian description and analysis of the LuGre friction model, Simul. Model. Pract. Theory 19 (3) (2011) 959–968.
[22] X. Jin, Y. Wang, Z. Huang, Approximately analytical technique for random response of LuGre friction system, Int. J. Non Linear Mech. 104 (2018) 1–7.
[23] D. Pikunov, A. Stefanski, Numerical analysis of the friction-induced oscillator of Duffing's type with modified LuGre friction model, J. Sound Vib. 440 (2019) 23–33.
[24] Z. Zhou, X. Zheng, Q. Wang, Z. Chen, Y. Sun, B. Liang, Modeling and simulation of point contact multibody system dynamics based on the 2D LuGre friction model, Mech. Mach. Theory (2021) 158 104244.
[25] F. Marques, Ł. Woliński, M. Wojtyra, P. Flores, H.M. Lankarani, An investigation of a novel LuGre-based friction force model, Mech. Mach. Theory 166 (2021), 104493.
[26] K.C. Valanis, A theory of viscoplasticity without a yield surface, Archiv. Mech. 23 (4) (1971) 517–551.
[27] K.C. Valanis, Fundamental consequences of a new intrinsic time measure. plasticity as a limit of the endochcronic theory, Archiv. Mech. 32 (1980) 171–191.
[28] L. Gaul, J. Lenz, Nonlinear dynamics of structures assembled by bolted joints, Acta Mech. 125 (1997) 169–181.
[29] L. Gaul, R. Nitsche, The Role of Friction in Mechanical Joints, Appl. Mech. Rev. 54 (2) (2001) 93–106.
[30] L. Gaul, U. Nackenhorst, K. Willner, J. Lenz, Nonlinear vibration damping of structures with bolted joints, in: Proceedings of SPIE—International Society for Optical Engineering; SPIE International Society for Optical Engineering: Bellingham, WA, USA, 1994, pp. 875–881.
[31] H. Ahmadian, H. Jalali, F. Pourahmadian, Nonlinear model identification of a frictional contact support, Mech. Syst. Sig. Process. 24 (8) (2010) 2844–2854.
[32] H. Jalali, H. Ahmadian, F. Pourahmadian, Identification of micro-vibro-impacts at boundary condition of nonlinear beam, Mech. Syst. Sig. Process. 25 (2011) 1073–1085.
[33] J. Abad, F.J. Medel, J.M. Franco, Determination of Valanis model parameters in a bolted lap joint: Experimental and numerical analyses of frictional dissipation, Int. J. Mech. Sci. 89 (2014) 289–298.
[34] E. Adeli, B. Rosic, H.G. Matthies, Identification of a Visco-plastic Model with Uncertain Parameters using Bayesian Methods, Int. J. Multiphase 75 (2018) 124–136.
[35] H. Ahmadian, H. Jalali, Identification of bolted lap joints parameters in assembled structures, Mech. Syst. Sig. Process. 21 (2007) 1041–1050.
[36] H. Ahmadian, H. Jalali, Generic element formulation for modelling bolted lap joints, Mech. Syst. Sig. Process. 21 (2007) 2318–2334.
[37] T. Naraghi, A.S. Nobari, A novel method for the identification of a model for the nonlinear characteristic of a bolted lap-joint, J. Vib. Control 23 (3) (2017) 484–500.
[38] H. Jalali, H. Ahmadian, J.E. Mottershead, Identification of nonlinear bolted lap-joint parameters by force-state mapping, Int. J. Solids Struct. 44 (2007) 8087–8105.
[39] D.J. Segalman, D.L. Gregory, M.J. Starr, B.R. Resor, M.D. Jew, J.P. Lauffer, N.M. Ames, Handbook on dynamics of jointed structures, Sandia National Laboratories, Albuquerque, 2009.
[40] X. Ma, L. Bergman, A. Vakakis, Identification of bolted joints through laser vibrometry, J. Sound Vib. 264 (3) (2011) 441–460.
[41] A.N. Tikhonov, Numerical methods for the solution of ill-posed problems, Kluwer Academic Publishers, Boston, 1995.
[42] X.G. Hua, Y.Q. Ni, J.M. Ko, Adaptive regularization parameter optimizationin output-error-based finite element model updating, Mech. Syst. Sig. Process. 2009 (23) (2009) 563–579.
[43] N. Jamia, H. Jalali, J. Taghipour, M.I. Friswell, H.H. Khodaparast, An equivalent model of a nonlinear bolted flange joint, Mech. Syst. Sig. Process. 153 (2021) 107–507.
[44] M.I. Friswell, J.E. Mottershead, Finite element modal updating in structural dynamics, Kluwer, Dordrecht, 1995.